**Proceedings of the ASME 2010 3rd Joint US-European Fluids Engineering Summer Meeting and 8th International Conference on Nanochannels, Microchannels, and Minichannels**
**FEDSM-ICNMM2010**
**August 1-5, 2010, Montreal, Canada**

**FEDSM-ICNMM2010-30414**

# RELIABILITY-BASED GLOBAL DESIGN OF SELF-ADAPTIVE MARINE ROTORS

**Michael R. Motley**
Dept. of Civil and Env. Eng.
Princeton University
Princeton, New Jersey 08544
Email: mmotley@princeton.edu

**Yin L. Young***
Dept. of Naval Arch. and Marine Eng.
University of Michigan
Ann Arbor, Michigan, 48109
Email: ylyoung@umich.edu

## ABSTRACT

Advanced composite materials are becoming more prevalent in marine applications, including marine rotors. Traditional rigid metallic marine rotors are highly optimized for a specific loading condition, away from which they tend to become sub-optimal. When properly designed, an adaptive composite marine rotor can provide improved performance through increased flexibility and hydroelastic tailoring of the structural deformations, allowing the blades to passively adapt to changing inflows through fluid-structure interactions. Because of the load-dependent deformations that an adaptive marine rotor will undergo, considerations must be made for variations in both propeller advance speed and rotational frequency that will affect hydrodynamic and structural performance. Through development of a probabilistic operational space, various rotor designs are considered herein in an effort to determine the appropriate loading condition to optimize the geometry and material configuration such that it maximizes the performance improvements. A sample set of geometries with varying material configurations and design speeds within the predicted design space are presented and analyzed over the probable range of operating conditions. A reliability-based global optimization technique is then presented to determine the optimal design point, geometry, and material configuration that maximizes hydroelastic performance over the range of anticipated flow conditions.

*Address all correspondence to this author.

## INTRODUCTION

The use of advanced composite materials in marine applications has increased in recent years in an effort to conserve weight, reduce maintenance costs, and increase survivability. Traditionally, marine rotors are constructed of rigid metallic alloys such as Nickel-Aluminum-Bronze (NAB) because of their superior corrosion resistance, high yield strength, and design characteristics. However, metallic propellers are optimized for a specific design condition and their inherent rigidity results in reduced performance under off-design conditions. Advanced composite materials, with proper optimization of the material and geometric design, can improve both hydrodynamic and structural performance through exploitation of the flexibility and bending-twisting coupling that allows for 3-D hydroelastic tailoring of the structural deformation. The flexibility of the composite material allows the rotor to passively adapt to changes in its surrounding flow environment through fluid-structure interactions (FSI). As such, the use of advanced composite materials has been shown to lead to improvements in overall performance of marine propellers by way of passive, load-dependent geometric tailoring that allows the pitch of the propeller blades to maintain the optimal angle of attack over a wider range of flow conditions, notably in off-design and in spatially/temporally varying flow conditions.

Utilization and exploitation of FSI has been under investigation in the aerospace industry for some time. Aeroelastic tailoring and optimization techniques have been shown to improve aeroelastic performance while reducing vibrations and loads for helicopter blades [1–3]. Similar approaches have been taken to improve performance and energy capture in wind turbines [4–6].

For marine applications, investigations on methodologies that use FSI have become more prevalent in recent years. Marine rotors, in general, experience consistent highly non-uniform flow fields because of geometric constraints and environmental variables such as boundary layer flow behind ship hulls, unsteady seas, and/or maneuvering. In addition, the increased density of water results in much higher loads and stresses that a marine rotor must resist compared to aerospace applications, and there also exists the potential for fluid cavitation. Hence, the capability to passively adapt to these changing flow conditions can be advantageous, particularly when operating at high rotational frequency in spatially varying flow. However, these rotors are more difficult to design and analyze than traditional rigid rotors because considerations must be made for the load-dependent FSI responses, material design, and potential material and/or instability failures. The performance of an adaptive composite marine rotor is directly dependent on the selection of a material and geometry design that satisfies the performance requirements. Selecting the most appropriate material and geometry design to maximize performance over the full range of expected operating conditions is not trivial because of the load-dependent deformation coupling behavior with multiple performance-based constraints.

Recent numerical [7–11] and experimental [12–14] investigations have demonstrated that properly designed self-adaptive rotors can achieve improved hydrodynamic performance and increased energy efficiency over a range of conditions when compared with an equivalent rigid rotor. The general design concept [10; 11] assumes that an optimal rigid geometry has been previously developed which is used as a basis for the design of the adaptive composite rotor. The adaptive composite rotor is then designed such that it performs equal to its rigid counterpart at the design advance coefficient, $J_a = J_o$, while it outperforms its rigid counterpart at off-design conditions, $J_a \neq J_o$. It is of note, however, that the performance of adaptive propellers is rate-dependent [10; 15]. Under fully-wetted flow conditions, rigid propeller performance depends only on the advance coefficient, $J_a = V_a/nD$. The load-dependent deformations, and thereby the hydroelastic performance, of adaptive composite propellers depend on both $J_a$ and propeller rotational frequency, $n$, (or similarly on advance speed, $V_a$, for a given propeller diameter $D$). In other words, for a geometrically similar rigid propeller, the non-dimensional hydrodynamic thrust and torque (or lift and drag) coefficients will be the same as long as the ratio of $V_a$ to $nD$, or $J_a$, is the same. For an adaptive propeller, however, the performance depends on the specific values of $V_a$ and $nD$, and not just the ratio, because the deformations depend on the total load. It should be noted that $V_a$ dictates the operating $J_a$, and hence $n$, because the propeller thrust must match the vessel resistance. As a result, a secondary design variable, herein defined as design advance speed, $V_o$, is needed for the design of adaptive composite propellers because of the load-dependent nature of the performance.

In its unloaded state, the adaptive composite propeller geometry is designed to be overpitched when compared with the rigid propeller. As it is loaded, the blades are designed to depitch as a function of the total load. Depending on the unloaded geometry of the adaptive propeller, variations in operating conditions result in a range of blade deformations (e.g. effective blade pitch angle distributions) across the design space. Over the range of the operating space, there must be a specific loading condition for which the deformed (loaded) adaptive propeller geometry and performance match those of its rigid counterpart to fairly compare the performance of the adaptive and rigid propellers. As such, the design advance speed, $V_o$, is defined as the speed at which the deformed adaptive propeller geometry must match with the rigid propeller geometry. Further, the optimal material configuration (e.g. laminate stacking sequence) will vary based on the design speed to allow for sufficient flexibility and to ensure material strength and stability. Hence, assuming that an optimal rigid propeller geometry has already been developed, optimization of an adaptive composite propeller requires selection of both a design advance speed, $V_o$, and a material configuration (e.g. stacking sequence) that maximizes propeller performance over the full range of expected operating conditions and not just at a single design condition.

### Objectives

The objective of this work is to develop a reliability-based global design procedure to optimize the performance of adaptive marine propellers over the full range of expected loading conditions. A series of geometry and material designs is presented and the resulting propeller efficiency, thrust, cavitation potential, and structural performance are compared over the range of operating conditions. Response surfaces are developed to represent the propeller performance based on numerical predictions using a 3-D propeller FSI analysis method. A load variation reduction-based objective function is presented and a Nelder-Mead constraint-based optimization technique is applied to the response surfaces to determine the optimal design advance speed and material stacking sequence to maximize propeller performance over the defined range of flow conditions based on the vessel resistance and speed characteristics.

## FORMULATION

A previously validated fully coupled 3-D potential-based boundary element method (BEM) and 3-D finite element method (FEM) is used to evaluate the steady-state and transient responses of both rigid and adaptive composite marine propellers under the range of expected loading conditions by computing the hydrodynamic blade loads, stresses, deformations, resonant frequencies, power demand, propulsive efficiency, and fluid cavitation potential. Details of the solver can be found in [9; 16]. In addition, the BEM-FEM solver is used to determine the unloaded geometry of the adaptive composite propeller, given a material stacking sequence, such that it deforms to match the optimized rigid propeller at a specified design load condition and to analyze each unloaded geometry over the expected operating conditions.

A critical assumption for the current design methodology is that an optimized rigid propeller geometry has already been determined such that it satisfies the performance requirements of the target vessel. Based on the optimized rigid propeller geometry, and for a given material configuration, the unloaded adaptive propeller geometry is determined iteratively such that the loaded propeller geometry and performance match with those of the rigid at the selected design condition, $J_o$ and $V_o$. The BEM-FEM solver takes approximately 30 minutes to perform a geometric design and approximately 3-5 minutes to analyze a given propeller at a specific loading condition on a single Intel processor. In order to optimize the propeller over the range of expected operating conditions, a series of loading conditions over the operational space is selected for analysis and a response surface is fitted to limit the number of simulations needed using the coupled 3-D BEM-FEM to reduce computational cost. The previously developed software package DACE [17] that applies a Kriging approximation is used to determine the optimization solution based on the response surfaces.

## DEVELOPMENT OF THE DESIGN SPACE

The optimization of any structure will be highly dependent on its application. An optimal design under one set of loading conditions may not be optimal under another. For a marine propeller operating behind a ship, the minimum requirement of the propeller is that it provides enough thrust to move the vessel through the water. Ship resistance, $R_T$, is defined as the force required to push a ship through the water at a constant ship velocity, $V_S$, and consists of components due to friction, waves, and air resistance among others, and is a function of hull geometry, ship speed, and fluid properties.

Because a propeller operates behind the hull of a ship, the total thrust required of the propeller includes not only ship resistance but also the additional frictional and pressure resistance caused by the presence of the hull. As such, more thrust is required when operating behind a hull compared with open-water (without the hull in unbounded water domain) tests to overcome the additional resistance caused by the presence of the hull. An empirical estimate of the additional thrust can be determined via the use of a thrust deduction factor, $t$, that can be defined through experimental testing or numerical simulations. The relationship between ship resistance, $R_T$ and required thrust, $T$, is defined as:

$$R_T = (1-t)T \tag{1}$$

Similarly, the presence of the hull changes the advance speed, $V_a$, of the water that reaches the propeller. A propeller operating in the wake of a hull will have different characteristics than a propeller operating in open water because of the viscous wake of the hull. As such, the fluid will be moving at a fraction of the ship speed, $V_S$, as the boundary layer effects from the hull change the local velocity of the water in the vicinity of the propeller. Hence, a similar relationship between the ship speed and the advance speed of the water at the propeller plane can be defined using an empirically derived wake fraction, $w$, where:

$$V_a = (1-w)V_S \tag{2}$$

Thus, for a given ship resistance curve, wake fraction, and thrust deduction factor, the required thrust, $T$, as a function of advance speed, $V_a$, can be derived.

It is intuitive that a ship resistance curve will be highly dependent on the geometry and the function of the ship, as well as on propulsor-hull interactions. For the purposes of demonstrating the design methodology, the required thrust is assumed to be a 5th-order polynomial function of the advance speed, which allows for the inclusion of a drag hump that would be typical for the resistance curve of a surface ship. The resistance curve, as shown in Figure 1, is assumed to be the mean of the ship resistance. Variables such as cargo weight, shallow or deep water, variations in sea state, or towing can create deviations in the required thrust. As such, to analyze the full range of potential operating conditions, upper and lower bounds are applied to the operational space. Herein, a linear increase in the deviation from the mean is applied to the resistance curve such that, at the top speed, $V_T$, the bounds represent a deviation from the mean of $\pm 15\%$.

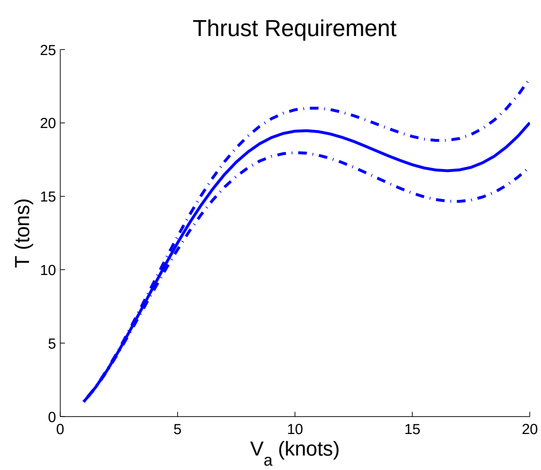


Figure 1. REQUIRED THRUST AS A FUNCTION OF THE ADVANCE SPEED BASED ON THE ASSUMED VESSEL RESISTANCE CHARACTERISTICS.

As previously noted, the general design concept for adaptive composite propellers assumes that its rigid counterpart has been previously optimized for the design advance coefficient, $J_D$, which corresponds to a specific design speed, $V_D$. Figure 2 shows the rigid propeller efficiency, $\eta$, as a function of the advance coefficient for a range of potential blade tip pitch angles; it shows how the rigid blade pitch angle is selected over the design space. Notice that the design advance speed of the rigid propeller is $J_D = 0.615$, which corresponds to the operating condition at the design speed of $V_D$=15 knots.

Based on the resistance curve shown in Figure 1 and the open water curves for the rigid propeller, the operating $J_a$ (and hence $n$) at each advance speed $V_a$ is selected as the point at which $T = R_T/(1-t) = \rho n^2 D^4 K_T$. Hence, the operating advance coefficient, $J_a$, can be expressed as a function of the advance speed, $V_a$, such that the thrust requirement is met, which provides the variation of the operating $J_a$ as a function of $V_a$, as shown in Figure 3. It should be noted that the upper and lower bounds of the operating $J_a$ in Figure 3 correspond to the lower and upper bounds, respectively, of the resistance curve shown in Figure 1.

Typically, a rigid propeller is designed to achieve the maximum efficiency at the speed most frequently expected over the lifetime of the vessel, i.e. $V_D = 15$ knots is the mode of the probability distribution function (PDF) of $V_a$, as shown in Figure 4. The PDF of $V_a$ is assumed to follow a Weibull distribution, with $V_D = 15$ knots and $V_T = 20$ knots, where $V_T$ is the speed for which the ship will operate at or below 95% of the time.

As shown in Figure 2, the blade pitch distribution (as represented by the blade tip pitch angle) of the rigid propeller is selected to optimize the propeller efficiency at $J_a = J_D = 0.615$, which corresponds to the operating condition for the most frequent advance speed, $V_a = V_D = 15$ knots. By performing a series of rigid blade computations at different pitch angle distributions, the variation of the efficiency with blade tip pitch angle, $\phi_{tip}$ and $J_a$, can be obtained. The results can then be used to determine the theoretical optimal pitch angle distribution as a function of $J_a$, as shown in Figure 2, which gives guidance on how to tailor the blade deformations (by controlling the deformed pitch) of the adaptive propeller to achieve the optimal performance over the full design space.

The design space of the propeller can be represented by the joint PDF of $J_a$ and $V_a$:

$$f_{J_a,V_a}(J_a,V_a) = f_{J_a}(J_a) f_{V_a}(V_a) \tag{3}$$

where $f_{J_a}(J_a) = P\{J_a \in dJ_a\}$ is the probability distribution of the advance coefficient (which can be determined using Figure 3) and $f_{V_a}(V_a) = P\{V_a \in dV_a\}$ is the probability distribution of the advance speed (as given in Figure 4). Figure 5 shows the joint PDF of the design space. Determination of the probabilistic design space is critical for the optimal design of an adaptive composite propeller because its load-dependent deformations depend not only on the advance coefficient but also of the advance speed, which dictates the total load acting on the blades.

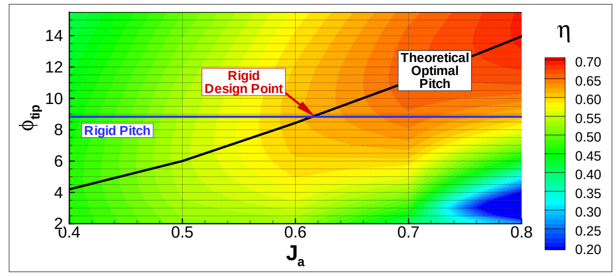


Figure 2. RIGID PROPELLER EFFICIENCY AS A FUNCTION OF ADVANCE COEFFICIENT AND BLADE TIP PITCH ANGLE.

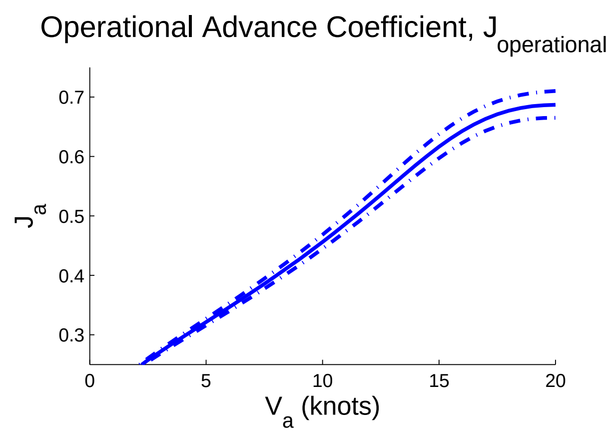


Figure 3. REQUIRED ADVANCE COEFFICIENT AS A FUNCTION OF THE ADVANCE SPEED BASED ON THE ASSUMED VESSEL RESISTANCE CHARACTERISTICS.

## COMPARISON OF ADAPTIVE PROPELLER GEOMETRIES

We have established that while a rigid propeller can be optimized for a specific design advance coefficient, $J_D$, the load-dependent and material-dependent deformation characteristics of an adaptive propeller require a design advance speed, $V_o$, for which we can determine the corresponding advance coefficient, $J_o(V_o)$, in addition to an optimal material configuration. Previous work by the authors [18] has shown that for a given material stacking sequence with $n$-layers, each of which has a primary fiber angle $\theta_n$ from the longitudinal axis of the blade, an equivalent single layer fiber angle, $\theta_{eq}$, can be determined for which approximately equal hydroelastic performance can be achieved. Hence, for hydroelastic optimization, the equivalent single layer fiber angle is used as a second design variable.

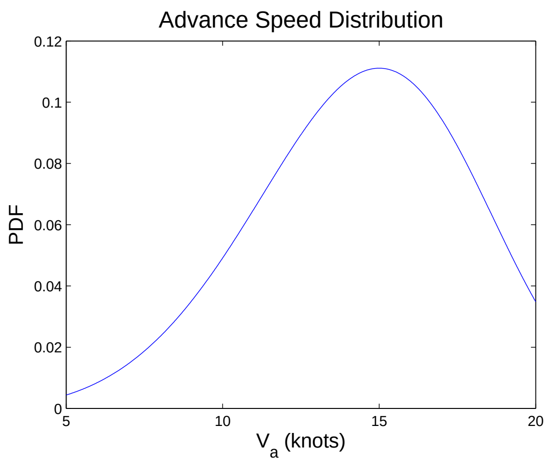


Figure 4. PROBABILITY DISTRIBUTION OF THE ADVANCE SPEED.

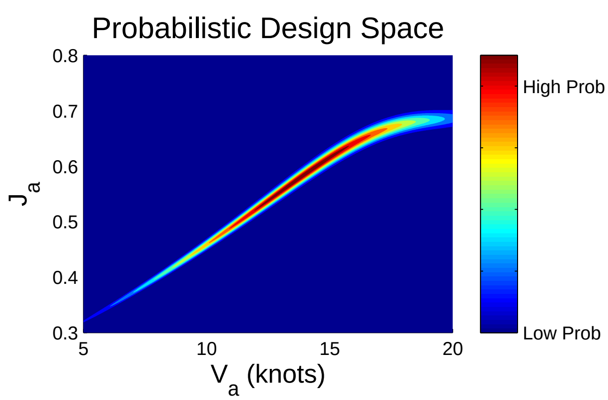


Figure 5. JOINT PDF OF THE EXPECTED OPERATIONAL SPACE.

For the purposes of this sample design, 24 potential geometries were examined to analyze the effects of various adaptive propeller design points. Design velocities of $V_o = [12, 14, 15, 16, 18, 20]$ knots were selected based on the PDF of the advance speed (Figure 4). The corresponding values of the advance coefficients could then be determined as $J_o = [0.521, 0.586, 0.615, 0.642, 0.676, 0.686]$. In addition, the range of potential equivalent single layer fiber angles is limited. For low values of $\theta_{eq}$, the blades become too stiff and do not deform enough to provide hydroelastic improvements over their rigid counterparts. On the other hand, for high values of $\theta_{eq}$, the blades become too flexible and the potential for structural strength and integrity issues becomes prevalent. Hence, values of $\theta_{eq} = [10.0, 12.5, 15.0, 17.5]^o$ were selected.

Using the BEM-FEM model, 24 unloaded geometries were developed. Figure 6 shows the contour of the unloaded tip pitch angles over the design space. The variation of the unloaded geometries (represented by the unloaded tip pitch angles) with $V_o$ correspond very closely to the resistance curve shown in Figure 1. The local minimum in the required thrust curve at approximately 16 knots corresponds to a local minimum in unloaded tip pitch angle at each specific $\theta_{eq}$ because the lower dimensional loading requires less depitching of the blade to reach the design condition. In addition, the unloaded tip pitch angle increases as $\theta_{eq}$ increases because, for low values of $\theta_{eq}$, the blades are stiff and do not have the capability to deform as much as when $\theta_{eq}$ is higher. Variations in unloaded tip pitch angle due as a function of $\theta_{eq}$ can be considered a measure of the blade's capacity to deform while variations due to $V_o$ are a function of the blade's necessity to deform.

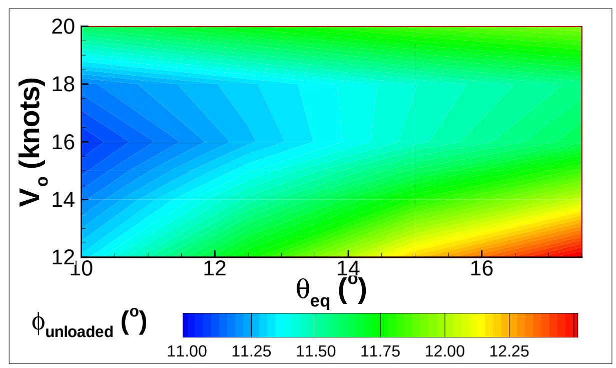


Figure 6. UNLOADED TIP PITCH ANGLE OF THE ADAPTIVE COMPOSITE PROPELLER OVER THE POTENTIAL DESIGN SPACE.

Given our set of potential geometries, a comparison of the propeller behavior over the design space is presented in Figures 7-9. Figure 7 shows a comparison of the deflected blade tip pitch angle for each design geometry over a range of flow conditions. Note that, for each of the designs, the adaptive propeller pitch matches with that of the rigid propeller at each $V_o$. The effect of $V_o$ on the overall deformation of the blades is quite evident. For $V_a < V_D$, $J_a < J_D$ (see Fig. 3) and thus the effective angle of attack is higher than the angle of attack at $V_D$. Hence, the adaptive blades tend to depitch more than the value at $V_D$, toward the theoretical optimal pitch angle, but the depitching action is limited because of the small dimensional load at small $V_a$. Alternatively, for $V_a > V_D$, $J_a > J_D$ and thus the angle of attack becomes smaller than the value at $V_D$. Hence, the adaptive blades tend to depitch less than the value at $V_D$, which is again toward the theoretical optimal pitch angle, but the effect is countered by the increase in total dimensional load at high $V_a$. Thus for some cases, the deformed tip pitch angle of the adaptive propeller is even further away from the theoretical optimal values than the rigid because of the load-dependent deformations. Moreover, it is evident via Figure 7 that the optimal $V_o$ is not necessarily equal to $V_D$.

Figure 8 shows a comparison of the deformed pitch angles

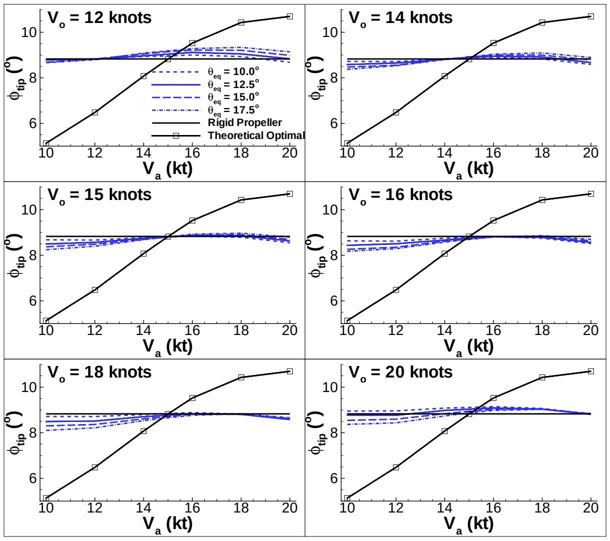


Figure 7. DEFORMED TIP PITCH ANGLE FOR THE VARIOUS ADVANCE SPEEDS AS A FUNCTION OF THE DESIGN VELOCITIES, $V_o$.

with the predicted cavitation bucket for $V_o = [12, 15, 20]$ knots. The dotted line crossing through the cavitation bucket represents the cavitation number, $\sigma_n$, of for the propeller at a depth of $h = 5$ m at different speeds, with $\sigma_n = (P_o - P_v)/\frac{1}{2}\rho n^2 D^2$. Cavitation occurs at $-C_P = (P_o - P)/\frac{1}{2}\rho n^2 D^2 \geq \sigma_n$ (i.e. $P \leq P_v$). Note that, except near the top speed, face side cavitation is not expected, while back side cavitation occurs at both high speeds and low speeds. It is of note, however, that improvements can be made which are directly related to the deformed pitch angle. By reducing the angle of attack at low $V_a$, the susceptibility to back side cavitation can be reduced. Similarly, an increased angle of attack at high values of $V_a$ reduces the susceptibility to face side cavitation. It is of note that certain designs result in increased susceptibility to face side cavitation at high speeds where the dimensional load that result from the high velocities forces the deformed pitch angle and resulting angle of attack to become lower than the rigid propeller. This is not as much the case for back side cavitation, as the blades tend to depitch below the rigid tip pitch angle for most of the designs with the exception being for low design speeds. Figure 9 shows a comparison of the hydroelastic performance of the propellers corresponding to Figure 8 in terms of thrust coefficient, $K_T$, and propeller efficiency, $\eta$. Because the deformed tip pitch angles of the adaptive propellers do not vary much from the rigid tip pitch angle, the efficiencies compare quite closely with the rigid for all of the designs. If we integrate the efficiency over the entire design space and weight it based on the joint PDF of the design space, we can see that there is, in general, a slight improvement in overall efficiency compared to the rigid propeller. Figure 10 shows a fitted surface of the overall efficiency improvement, $\Delta\eta_{total}$, where:

$$\Delta\eta_{total} = \frac{\int_{J_a}\int_{V_a}\left[\eta_{adaptive}(J_a,V_a)\, f_{J_a,V_a}(J_a,V_a)\right] dJ_a dV_a}{\int_{J_a}\int_{V_a}\left[\eta_{rigid}(J_a,V_a)\, f_{J_a,V_a}(J_a,V_a)\right] dJ_a dV_a} - 1 \quad (4)$$

It is more notable that, for lower pitch, the lower angle of attack results in lower thrust coefficients, while the opposite is true for higher pitch angles. The significance of this is that the range of loads, and the resulting range of stresses, that the adaptive blades will experience is lower than those experienced by the rigid propeller. This is critical for considering the fatigue behavior of the two structures, as fatigue life is highly dependent on the amplitude of stress variations over the life of the structure, thus for unsteady loading conditions, the improvements provided by the adaptive propeller can be expected to be notable. In addition to unsteady flows, this can become critical in spatially or temporally varying flows, particularly when related to fatigue, because the cyclic load variation with each revolution, and thereby reduction of the load variations, can extend the fatigue life of the structure.

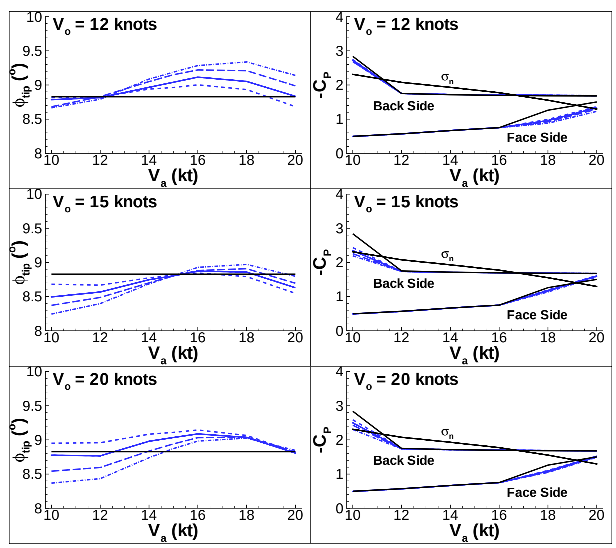


Figure 8. COMPARISON OF THE DEFORMED TIP PITCH ANGLE (LEFT) WITH THE CAVITATION POTENTIAL (RIGHT) FOR VARIOUS DESIGN ADAPTIVE PROPELLER GEOMETRIES. THE LINE LEGEND FOLLOWS THAT OF FIGURE 7.

## PROPELLER OPTIMIZATION

We have shown in the previous section that, given an appropriately designed adaptive composite propeller, hydroelastic

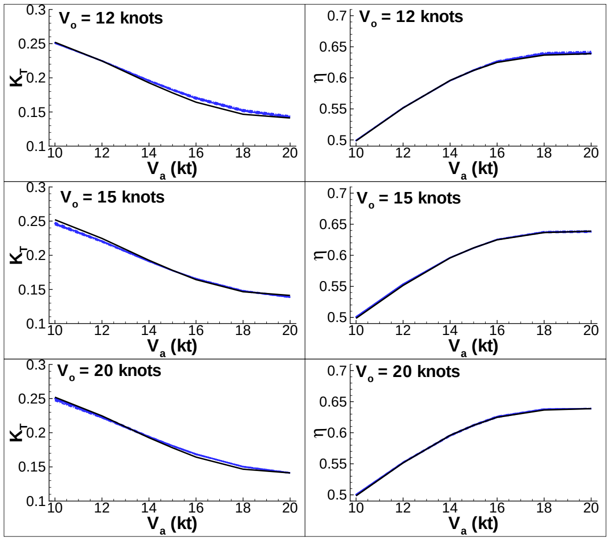


Figure 9. COMPARISON OF THE THRUST COEFFICIENT (LEFT) AND PROPELLER EFFICIENCY (RIGHT) FOR VARIOUS DESIGN ADAPTIVE PROPELLER GEOMETRIES. THE LINE LEGEND FOLLOWS THAT OF FIGURE 7.

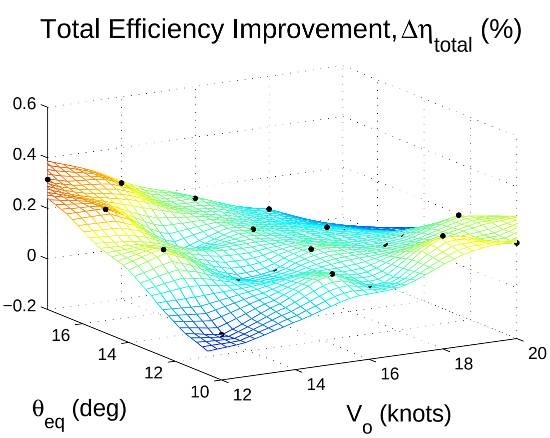


Figure 10. TOTAL PROBABILISTIC EFFICIENCY IMPROVEMENT OVER THE DESIGN SPACE.

performance improvements can be achieved over its rigid counterpart in terms of cavitation potential (both face and back side), propeller efficiency, and load variations. If we assume that the rigid propeller is optimized for the most frequent operating condition, then, for comparative purposes, the adaptive propeller should be optimized such that it maximizes hydroelastic performance improvements over the entire expected operational space. It is of note, however, that we cannot maximize one aspect of performance without potentially reducing the improvements for another aspect of performance, and hence it is necessary to determine, based on the application of the structure and on the potential for improvement, what the objective function and constraints of the optimization should be.

We have shown in Figure 10 that the total probabilistic efficiency improvement ranges from approximately -0.1%-0.5%. While the improvements are slight, over the life of the structure this will provide some benefit; however, the potential for improvement is low enough that it is not practical to optimize the propeller for maximum efficiency improvement. Hence, we can define an efficiency constraint function, $c_1(J_a, V_a)$, that requires that the adaptive propeller provides overall efficiency improvement over its rigid counterpart:

$$c_1(J_a, V_a) = \Delta\eta_{total} \geq 0 \tag{5}$$

In addition, susceptibility to cavitation, both face and back side, can be reduced by properly selecting a design point. It is of note, however, that these improvements occur more toward the tails of the advance speed PDF. At and around the most probable advance speed, $V_D$, the potential for cavitation for the adaptive propeller is approximately the same as that of the rigid propeller. If we compare where the cavitation buckets intersect with the cavitation number, however, it is evident that the adaptive propeller can extend the cavitation free region around $V_D$. The probability of cavitation occurring can be determined by comparing the front and back side pressure coefficients, the cavitation number, and the probabilistic design space, and a Bernoulli distribution can be formulated such that:

$$\begin{aligned}(P_{cav})_{face}(J_a, V_a) &= 1, \; -(C_P)_{face}(J_a, V_a) - \sigma_n(J_a, V_a) > 0 && (6)\\ &= 0, \; -(C_P)_{face}(J_a, V_a) - \sigma_n(J_a, V_a) < 0 \\ (P_{cav})_{back}(J_a, V_a) &= 1, \; -(C_P)_{back}(J_a, V_a) - \sigma_n(J_a, V_a) > 0 && (7)\\ &= 0, \; -(C_P)_{back}(J_a, V_a) - \sigma_n(J_a, V_a) < 0\end{aligned}$$

The susceptibility for cavitation can then be defined by integrating the probability of cavitation over the design space:

$$(P_{cav})_{face} = \int_{J_a}\int_{V_a} \left[(P_{cav})_{face}(J_a, V_a)\, f_{J_a,V_a}(J_a, V_a)\right] dJ_a dV_a \tag{8}$$

$$(P_{cav})_{back} = \int_{J_a}\int_{V_a} \left[(P_{cav})_{back}(J_a, V_a)\, f_{J_a,V_a}(J_a, V_a)\right] dJ_a dV_a \tag{9}$$

Thus we can define this as a set of cavitation potential constraint functions, $c_2(J_a, V_a)$ and $c_3(J_a, V_a)$, that require that the adaptive propeller reduces the susceptibility to both face and back side cavitation over the design space:

$$c_2(J_a, V_a) = \frac{\left((P_{cav})_{face}\right)_{adaptive}}{\left((P_{cav})_{face}\right)_{rigid}} - 1 < 0 \tag{10}$$

$$c_3(J_a,V_a) = \frac{((P_{cav})_{back})_{adaptive}}{((P_{cav})_{back})_{rigid}} - 1 < 0 \quad (11)$$

With the three constraint functions defined, we then define an objective function, $g_{obj}$, such that we minimize the load variations, as defined by the thrust coefficient, $K_T$ (Figure 9), and in turn reduce the amplitude of the stress fluctuations and susceptibility to cavitation that would be expected under unsteady operating conditions. As mentioned above, by reducing the stress fluctuations, it can be expected that we can extend the fatigue life of the structure in spatially or temporally varying flows. Continuing to use the rigid propeller performance as a baseline, we can define an objective function to select a design point that minimizes the variation in $K_T$:

$$g_{obj}(V_o,\theta_{eq}) = \min_{V_o,\theta_{eq}} \frac{(|\Delta K_T|)_{adaptive}}{(|\Delta K_T|)_{rigid}} \quad (12)$$

subject to the three constraint functions defined above.

With an objective function and constraints defined, selection of an appropriate optimization procedure is necessary. Because of the number of points needed in the design space in addition to the iterative nature of the BEM-FEM model, a gradient-free optimization procedure is applied herein. The Nelder-Mead simplex or nonlinear simplex method [19] is selected for the optimization for this design example because it does not require the computation of derivatives and it does not require the objective function to be smooth. While the Nelder-Mead method becomes weak for a larger number of design variables, for the two-variable optimization shown here it is efficient. Because we are using a gradient-free optimization scheme, the constraints are implemented directly into the objective function as an infinite penalty function, $\hat{c}(J_a,V_a)$, where for a system with $j$ constraints:

$$\hat{c}_j(J_a,V_a) = \infty \text{ if the constraint } c_j(J_a,V_a) \text{ is violated} \quad (13)$$
$$= 0 \text{ otherwise}$$
$$\hat{c}(J_a,V_a) = \max_j \hat{c}_j(J_a,V_a) \quad (14)$$

and we can define a modified objective function, $\pi_{obj}$ as:

$$\pi_{obj}(J_a,V_a) = g_{obj}(J_a,V_a) + \hat{c}(J_a,V_a) \quad (15)$$

and the optimizer will tend toward only feasible values that have not been forced to infinity by the penalty function and thus we can develop a feasible design space. Figure 11 shows a plot of the feasible design space based on each of the individual constraints as well as a cumulative feasible design space considering all of the constraints. The black regions are feasible design points while the white regions are not feasible. The back side cavitation constraint only comes in for lower design speeds where the adaptive and rigid propeller angles of attack are very close, by design, at the low speeds where back side cavitation occurs. Similarly, for adaptive design speeds between 15-19 knots, the adaptive propeller angle of attack is consistently near or below the rigid propeller angle of attack at high speeds because of velocity-induced deformations, resulting in increased face side cavitation for those designs. The efficiency constraint, on the other hand, places very little constraint on the design as only stiff propellers designed for low speeds or flexible propellers designed for high speeds are considered not feasible. For stiff propellers at a low design speed, there is neither capability nor necessity for initial overpitching of the propeller and at high speeds the propeller tends to depitch beyond the rigid pitch angle. The opposite is true for overly flexible propellers at high design speeds, where the initial overpitch is high and at low speeds the blades do not depitch enough to provide improvement over the rigid propeller. Given the three constraints, the cumulative feasible design space is shown in the bottom right corner of Figure 11.

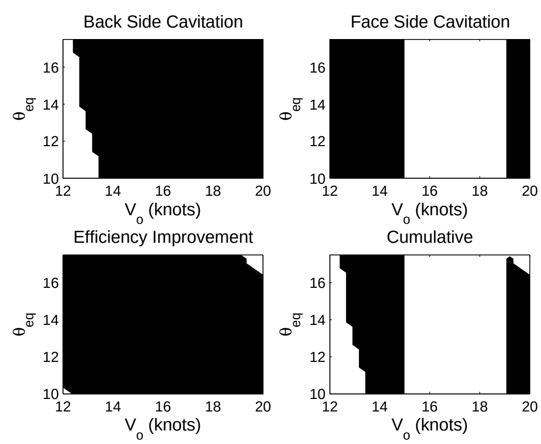


Figure 11. FEASIBLE (BLACK) AND NON-FEASIBLE (WHITE) DESIGN SPACE BASED ON BACK SIDE CAVITATION (TOP LEFT), FACE SIDE CAVITATION (TOP RIGHT), EFFICIENCY (BOTTOM LEFT), AND CUMULATIVE (BOTTOM RIGHT) CONSTRAINTS.

With the feasible design space defined, a comparison can be made between the objective and the modified objective functions, as shown in the contour maps of Figure 12. By running the optimizer in the constrained space, we can converge to the global minimum within the design space and have a feasible design point that minimizes the variation in thrust coefficient while meeting the cavitation and efficiency constraints. For this design, the optimal design point was found to be $V_o = 13.0$ knots and $\theta_{eq} = 17.25^o$. It is of note that there exists a second minimum at approximately $V_o = 19.2$ knots and $\theta_{eq} = 17.5^o$. Because the Nelder-Mead simplex method does not guarantee that a global minimum will be found, several starting points that sample the design space were used for the original simplex and the two local minima are compared. Figures 13 and 14 show sample paths of the simplexes as they converge to the minima and how the selection of the starting point and size of the initial simplex can affect the optimization. The point $V_o = 13.0$ knots and $\theta_{eq} = 17.25^o$ was found to provide the biggest improvement of approximately 9.9% reduction in variation of the thrust coefficient when compared with the rigid. Correspondingly, the probability of back side cavitation was reduced by 2.3% while the probability of face side cavitation was reduced by 9.7%. In addition, the total efficiency improvement was found to be approximately 0.3% over the design space.

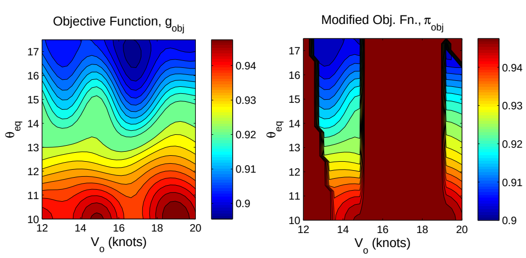


Figure 12. CONTOUR MAP OF THE OBJECTIVE FUNCTION WITHOUT CONSTRAINTS (LEFT) AND THE MODIFIED OBJECTIVE FUNCTION WITH CONSTRAINTS INCLUDED (RIGHT).

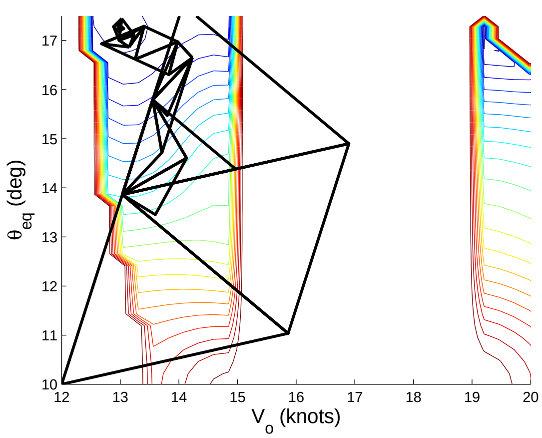


Figure 13. CONVERGENCE OF THE NONLINEAR SIMPLEXES TO THE *GLOBAL* MINIMUM OF THE MODIFIED OBJECTIVE FUNCTION.

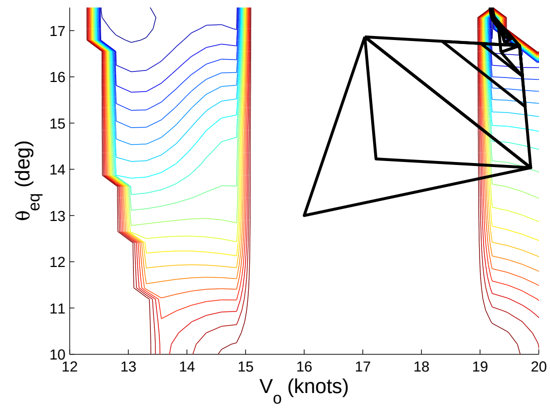


Figure 14. CONVERGENCE OF THE NONLINEAR SIMPLEXES TO THE *LOCAL* MINIMUM OF THE MODIFIED OBJECTIVE FUNCTION.

## CONCLUSION AND SUMMARY

This work presents a reliability-based global design optimization methodology for adaptive marine propellers operating under a range of steady loading conditions. Given a ship resistance curve and optimized rigid propeller geometry, in addition to a probability distribution of the propeller advance speed, a probabilistic operational space was developed within which the adaptive propeller can be expected to operate. Because of the rate-dependent deformation behavior of adaptive marine structures, developing a realistic operational envelope is critical because propeller performance depends on the total dimensional load, which is a function of $V_a$ and $J_a$. Hence, not only does the material configuration have to be optimized for an adaptive marine structure, but selecting the appropriate design speed for which the adaptive propeller geometry and performance will match those of the rigid propeller becomes a critical design variable.

Using a previously validated BEM-FEM model, a set of sample geometries were designed and analyzed with varying material configurations and design speeds over the expected operational space. The resulting geometries vary depending on velocity dependent load requirements and the flexibility provided by the material configuration. Comparisons of the various geometries show that selecting the appropriate design point that maximizes performance is not trivial. By comparing the structural deformations, efficiencies, thrust coefficients, and potential for cavitation, it is evident that an appropriately designed adaptive propeller can improve various aspects of hydrodynamic performance but that, in general, maximizing performance in one area can result in decreased performance in others.

The hydrodynamic performance of the various designs was analyzed over the design space and the propeller design was optimized based on minimization of the variation in the thrust coefficient over the operational space. Minimization of the thrust coefficient is representative of minimizing the amplitude of load variation and correspondingly stress variation and potential for cavitation that the propeller blades will see over the life of the structure. This is critical to extending the fatigue life of the blades and to extend the range of cavitation free operations. Constraints were placed on the optimization such that, compared with the rigid propeller, the adaptive propeller was, on average, more efficient and less susceptible to cavitation. Using a Nelder-Mead simplex optimization scheme with penalty constraints, an optimal design point of $V_o = 13.0$ knots and $\theta_{eq} = 17.25^o$ was found that reduces the load variation by approximately 10%, cavitation potential by 2.3% on the back side and 9.7% on the face side, and increases the total efficiency by approximately 0.3%.

Overall, this work stresses the importance of considering the effects of load-dependent deformations when designing an adaptive marine structure. These effects create additional design variables that must be considered and make the determination of what is the optimal adaptive design highly non-trivial. The optimization presented herein is based only on hydrodynamic performance. Further considerations must be made based on structural performance to ensure that structural strength and/or stability issues do not become a concern. Additionally, the results presented herein are for steady state operation. For unsteady applications, the improvements provided by the adaptive propeller are expected to become more noticeable in terms of reduction of loads, delay of cavitation, and improved hydrodynamic efficiency.


## ACKNOWLEDGMENTS

The authors are grateful to the Office of Naval Research (*ONR*) and Dr. Ki-Han Kim (program manager) for their financial support through grant numbers N00014-09-1-1204 and N00014-10-1-0170.


## REFERENCES


[1] Ganguli, R., and Chopra, I., 1997. “Aeroelastic tailoring of composite couplings and blade geometry of a helicopter rotor using optimization methods”. *Journal of American Helicopter Society,* **42**(3), pp. 218–228.

[2] Soykasap, O., and Hodges, D., 2000. “Performance enhancement of a composite tilt-rotor using aeroelastic tailoring”. *Journal of Aircraft,* **37**, pp. 850–858.

[3] Glaz, B., Friedmann, P., and Lu, L., 2009. “Helicopter vibration reduction throughout the entire flight envelope using surrogate-based optimization”. *Journal of American Helicopter Society,* **54**(1), p. 012007.

[4] Lee, A., and Flay, R., 2000. “Compliant blades for passive power control of wind turbines”. *Wind Engineering,* **24**, pp. 3–11.

[5] Lobitz, D., and Veers, P., 2003. “Load mitigation with bending/twist-coupled blades on rotors using modern control strategies”. *Wind Energy,* **6**, pp. 105–117.

[6] Maheri, A., and Isikveren, A., 2009. “Performance prediction of wind turbines utilizing passive smart blades: approaches and evaluation”. *Wind Energy,* **13**, pp. 255–265.

[7] Lee, Y., and Lin, C., 2004. “Optimized design of composite propeller”. *Mechanics of Advanced Materials and Structures,* **11**, pp. 17–30.

[8] Lin, C., and Lee, Y., 2004. “Stacking sequence optimization of laminated composite structures using genetic algorithm with local improvement”. *Composite Structures,* **63**, pp. 339–345.

[9] Young, Y., 2008. “Fluid-structure interaction analysis of flexible composite marine propellers”. *Journal of Fluids and Structures,* **24**(6), pp. 799–818.

[10] Motley, M., Liu, Z., and Young, Y., 2009. “Utilizing fluid-structure interactions to improve energy efficiency of composite marine propellers in spatially varying wake”. *Composite Structures,* **90**(3), pp. 304–313.

[11] Liu, Z., and Young, Y., 2009. “Utilization of bending-twisting coupling effects for performance enhancement of composite marine propellers”. *Journal of Fluids and Structures,* **25**, pp. 1102–1116.

[12] Gowing, S., Coffin, P., and Dai, C., 1998. “Hydrofoil cavitation improvements with elastically coupled composite materials”. In Proceeding of 25th American Towing Tank Conference.

[13] Chen, B., Neely, S., Michael, T., Gowing, S., Szwerc, R., Buchler, D., and Schult, R., 2006. “Design, fabrication and testing of pitch-adapting (flexible) composite propellers”. In The SNAME Propellers/Shafting Symposium ’06.

[14] Lin, C., Lee, Y., and Hung, C., 2009. “Optimization and experiment of composite marine propellers”. *Composite Structures,* **89**, pp. 206–215.

[15] Young, Y., and Motley, M., 2009. “Rate-dependent hydroelastic response of self-adaptive composite propellers in fully wetted and cavitating flows”. In Proceedings of the 7th International Symposium on Cavitation (CAV2009).

[16] Young, Y., 2007. “Time-dependent hydroelastic analysis of cavitating propellers”. *Journal of Fluids and Structures,* **23**, pp. 269–295.

[17] Lophaven, S., Nielsen, H., and Sondergaard, J., 2002. DACE - A MATLAB Kriging Toolbox. Technical Report IMM-TR-2002-12. Tech. rep., Technical University of Denmark.

[18] Young, Y. L., Liu, Z., and Motley, M., 2008. “Influence of material anisotropy on the hydroelastic behaviors of composite marine propellers”. In 27th Symposium on Naval Hydrodynamics.

[19] Nelder, J., and Mead, R., 1965. “Simplex method for function minimization”. *Computer Journal,* **7**, pp. 308–313.